

# Mineralogical Microheterogeneity Formed via Dissimilatory Iron Reduction

C. M. Hansel,<sup>1</sup> S. G. Benner,<sup>1</sup> S. Fendorf,<sup>1</sup> S. Sutton,<sup>2</sup> M. Newville,<sup>2</sup> T. Trainor<sup>2</sup>  
<sup>1</sup>Department of Geological and Environmental Sciences, Stanford University, Stanford, CA, U.S.A.  
<sup>2</sup>Argonne National Laboratory, Argonne, IL, U.S.A.

## Introduction

Iron is commonly a master variable that defines the fate of trace element contaminants. The importance of microorganisms in the biogeochemical cycling of Fe is well recognized [1]. Dissimilatory iron-reducing bacteria (DIRB), which are ubiquitous in aquatic soils and aquifers, couple the oxidation of organic matter or H<sub>2</sub> to the reduction of various Fe(III) oxide phases. We have recently observed that the reaction products following microbial reduction of two-line ferrihydrite under dynamic-flow conditions are goethite and magnetite [2]. The distribution of goethite and magnetite vary spatially and temporally, corresponding primarily with Fe(II) concentration gradients [1-4].

The presence of multiple mineral phases is often observed in natural systems. The occurrence of complex secondary mineral assemblages cannot be explained by homogeneous thermodynamic calculations and is likely the product of spatial and/or temporal variability. Quantifying the scale of mineral phase heterogeneity can lend insight into the mechanism of formation, provide a framework for further geochemical evolution, and assist in predicting contaminant behavior within this complex system. Additionally, knowing the scale of heterogeneity is beneficial for selecting the appropriate investigative approach. Accordingly, here we investigate the microheterogeneity and relationships of the secondary precipitates magnetite and goethite following dissimilatory iron reduction of two-line ferrihydrite [2]. Grains were analyzed by using scanning electron microscopy (SEM) and micro-x-ray absorption spectroscopy ( $\mu$ -XAS). Coupling of SEM and  $\mu$ -XAS provides insight into the microheterogeneity of secondary mineral phases on the surface of ferrihydrite.

## Methods and Materials

We examined microbially induced Fe mineral transformations of ferrihydrite-coated Si sand by using *Shewanella putrefaciens* strain CN32 (hereinafter referred to as CN32) in an artificial groundwater medium under advective flow (see Ref. 2 for experimental details). Three columns were terminated at 2, 4, and 16 d to obtain a time-series of solid-phase evolution. Upon termination, the solids were extracted and homogenized at 2-cm intervals along the length of the column. Bacteria were enumerated by using plate counts. Solution samples were

obtained from both the effluent and side sampling ports and analyzed for lactate, acetate, and Fe(II) concentration by colorimetric and ion chromatographic techniques.

X-ray absorption spectroscopy was performed on beamline 13-ID-C at the APS. X-ray absorption near-edge structure (XANES) analysis was conducted by using WinXAS. Spectra were background subtracted by using a low-order polynomial function and normalized by setting the total atomic cross-sectional absorption to unity. The first derivative of each spectrum was obtained by using a Savitzky-Golay algorithm, and Fe speciation was determined by noting the main-edge peak position in the first-derivative curve. Linear fitting routines were used to reconstruct the unknown by using a set of reference Fe standards in order to determine the relative percentages of mineral phases within the samples. Model Fe compounds used in spectral fitting routines include iron sulfide (FeS), siderite (FeCO<sub>3</sub>), ferrihydrite (Fe(OH)<sub>3</sub>•nH<sub>2</sub>O), goethite ( $\alpha$ -FeOOH), lepidocrocite ( $\gamma$ -FeOOH), hematite ( $\alpha$ -Fe<sub>2</sub>O<sub>3</sub>), green rust (Fe<sup>II</sup><sub>6-x</sub>Fe<sup>III</sup><sub>x</sub>(OH)<sub>12</sub>[(SO<sub>4</sub>)<sub>x/2</sub>•3H<sub>2</sub>O]), and magnetite (Fe<sub>3</sub>O<sub>4</sub>).

Samples for SEM were dispersed anaerobically onto carbon-coated Cu grids and analyzed by using a Philips XL30 field emission SEM (Pacific Northwest National Laboratory) fitted with backscatter and secondary electron detectors and an IMIX energy-dispersive x-ray analytical system.

## Results

Microbial reduction of two-line ferrihydrite under advective flow results in the secondary mineralization of goethite and magnetite [2]. The concentrations and distribution of goethite and magnetite precipitates vary within the column. While goethite has a uniform distribution both spatially and temporally, magnetite increases both downgradient and over time (bulk extended x-ray absorption fine structure [EXAFS] data not shown). Upon reaching steady state, magnetite is the dominant (88%) sink for Fe(II), as well as an appreciable (29%) secondary source of Fe(III), within the system. Moreover, goethite sequesters about 16% of the Fe(III) after 16 d of reduction.

The physicochemical properties of goethite and magnetite vary considerably. The sorption capacity of goethite and magnetite is substantially lower than that of ferrihydrite. Moreover, magnetite may serve as a potential reductant within the system. Thus, the distribution of the

mineral phases may correspond with development of microenvironments on individual grains. Additionally, following 16 d, reduction declines appreciably, yet 87% of the original Fe(III) within the column is still available for reduction (data not shown). Similarly, 48% of the original ferrihydrite remains within the column. Since both goethite and magnetite are less bioavailable for microbial reduction, their distribution may lend insight into the means of cessation of microbial reduction. Accordingly, the distribution and microheterogeneity of solid-phase precipitates were investigated by using SEM and  $\mu$ -XAS. Micro-XANES spectra were obtained along a 300- $\mu\text{m}$  transect at 5- $\mu\text{m}$  intervals of a single Fe-coated Si sand grain (Fig. 1). Iron has a patchy distribution on the sand grains. First-derivative XANES spectra illustrate appreciable changes along the 300- $\mu\text{m}$  transect (Fig. 2). Three dominant peaks are observed in the first-derivative spectra at 7120, 7123, and 7127 eV. Comparison of first-derivative XANES spectra of ferrihydrite, goethite, and magnetite standards reveals a peak (7120 eV) unique to magnetite (Fig. 3). Magnetite, being a mixed-valence (ferrous/ferric) mineral, contains spectral contributions from both ferrous and ferric iron. The peak at 7120 eV, which is not observed in the ferric hydroxides ferrihydrite or goethite, is due to the presence of ferrous iron within the magnetite structure. The appearance of magnetite regions along the XANES transect is therefore apparent by monitoring the spectral features at 7120 eV. A number of small regions ( $\sim 10$  to  $\sim 20$   $\mu\text{m}$ ) containing magnetite are found adjacent to those lacking appreciable (5%) magnetite.

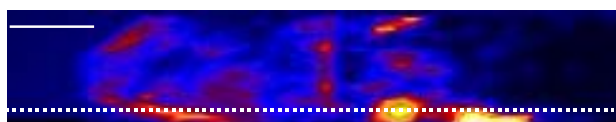


FIG. 1. X-ray fluorescence microprobe image depicting the distribution of Fe on a Si sand grain. The scale bar (solid white line) represents 40  $\mu\text{m}$ . The transect used for XANES spectra collection is illustrated by the dotted white line.

Changes in mineral fractions were determined by obtaining linear-combination fits to the first-derivative XANES spectra. Fits along the transect further illustrate the microheterogeneity of the secondary precipitates. Regions containing ferrihydrite and magnetite are found adjacent to ferrihydrite- and goethite-bearing regions (Fig. 4). Effectively, goethite- and magnetite-bearing regions do not coincide, suggesting that the two secondary minerals compete for the ferrihydrite surface. This corresponds with the plausible mechanisms of

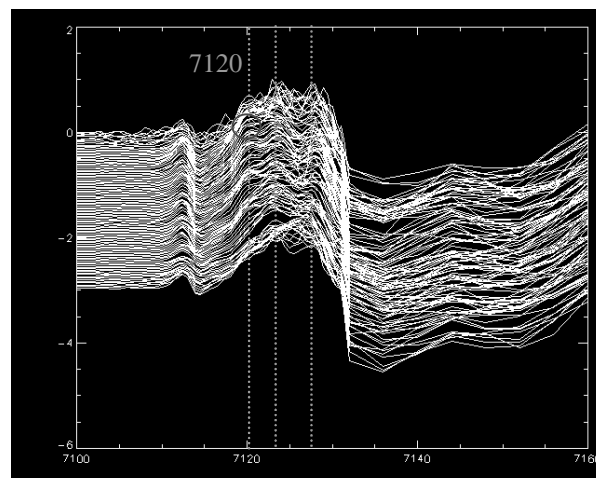


FIG. 2. XANES spectra obtained along a 300- $\mu\text{m}$  transect depicted in Fig. 1. XANES spectra were obtained every 5  $\mu\text{m}$ . The peak at 7120 eV is indicative of magnetite. Red circle illustrates region of spectra indicated in Fig. 4.

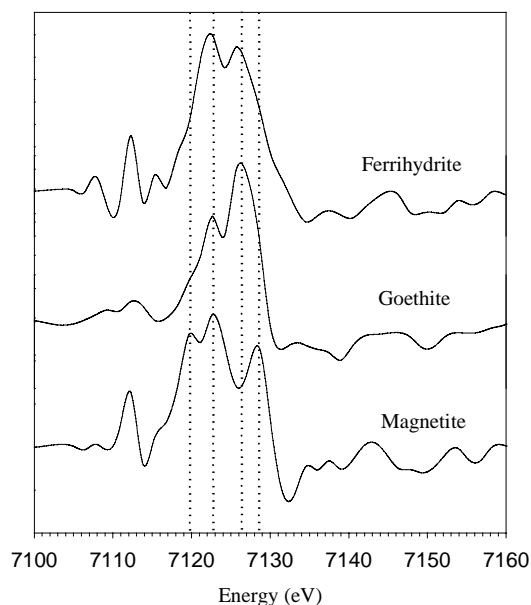


FIG. 3. XANES spectra for ferrihydrite, goethite, and magnetite standards. Dotted lines indicate dominant peaks within spectra.

mineralization. Goethite forms by either aggregation-based crystal growth or Ostwald ripening of ferrihydrite (dissolution/reprecipitation) [5-6]. Magnetite nucleation also depends on ferrihydrite, forming via a solid-state transformation of ferrihydrite [7].

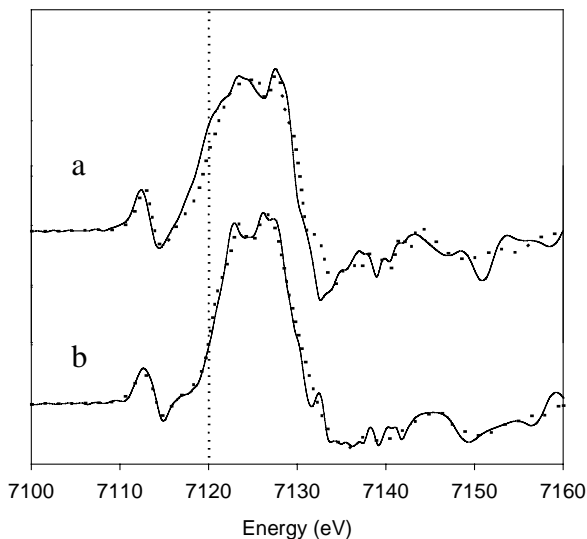


FIG. 4. XANES spectra (solid line) and linear combination fits (dotted) of two adjacent points (see red circle in Fig. 2) along a transect (Fig. 1). Fits indicate that (a) consists of 57% magnetite and 43% ferrihydrite, while (b) contains 90% ferrihydrite and 10% goethite. Fits are  $\pm 5\%$ .

SEMs reveal the small particle size of the secondary precipitates and confirm the phase heterogeneity on the ferrihydrite surface (Fig. 5). Magnetite averages 50 nm in diameter with a botryoidal morphology. Goethite crystals average 10 nm in width and 100 nm in length and have a lathe-like crystal habit. Isolated patches of goethite and magnetite precipitates are evident within the micrographs.

Coupled  $\mu$ -XAS and SEM illustrate the scale of heterogeneity in secondary minerals produced during dissimilatory reduction of two-line ferrihydrite. While the individual particle sizes of magnetite and goethite are less than 100 nm, the two phases exist in larger uniform patches ( $<20 \mu\text{m}$ ). The microheterogeneity of goethite and magnetite implies the existence of microenvironments at the ferrihydrite surface during secondary mineralization. Discrete phase regions may maintain the presence of microenvironments and differential regions of sorption and/or reduction processes. The sorption and reducing capacity, as well as the bioavailability of phases, vary dramatically on the scale of a few micrometers. Thus, the results of this research further exemplify the significance of microenvironments in secondary mineralization.

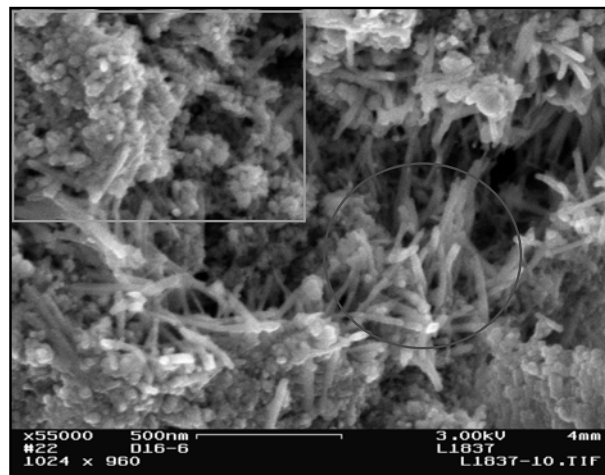


FIG. 5. SEM image of the 16-d reaction solids illustrating the microheterogeneity of goethite (red circle) and magnetite (green rectangle) phases.

## Acknowledgments

This research was supported by the U.S. Department of Energy (DOE), Office of Biological and Environmental Research (BER), Natural and Accelerated Bioremediation Research (NABIR) Program under Grant No. DE-FG03-00ER63029. Use of the APS was supported by the DOE Office of Science, Office of Basic Energy Sciences, under Contract No. W-31-109-ENG-38. The research was performed on the GeoSoilEnviro Consortium for Advanced Radiation Sources (GSECARS) beamline 13-ID-C. SEM images were obtained at the Environmental Molecular Sciences Laboratory (EMSL), Pacific Northwest National Laboratory.

## References

- [1] D. R. Lovley, *Microbiol. Rev.* **55**, 259-287 (1991).
- [2] S. G. Benner et al., *Environ. Sci. Technol.* **36**, 1705-1711 (2002).
- [3] J. K. Fredrickson et al., *Geochim. Cosmochim. Acta* **62**, 3239-3257 (1998).
- [4] J. M. Zachara et al., *Geomicrob. J.* **19**, 179-208 (2002).
- [5] J. F. Banfield et al., *Science* **289**, 751-754 (2000).
- [6] R. M. Cornell and U. Schwertmann, *The Iron Oxides: Structure, Properties, Reactions, Occurrences, and Uses*, (VCH [now WILEY-VCH Weinheim, Berlin, Germany] 1996).
- [7] S. Ardizzone and L. Formaro, *Mater. Chem. Phys.* **8**, 125-133 (1983).